Eur. Phys. J. C 51, 645–657 (2007)
DOI 10.1140/epjc/s10052-007-0319-2

THE EUROPEAN PHYSICAL JOURNAL C

Regular Article – Theoretical Physics

High-loop perturbative renormalization constants for lattice QCD (I): finite constants for Wilson quark currents

F. Di Renzo[1], V. Miccio[2], C. Torrero[3], L. Scorzato[4,a]

[1] Dipartimento di Fisica, Università di Parma and INFN, Gruppo Collegato di Parma, viale G.P. Usberti 7/a, 43100 Parma, Italy
[2] I.N.F.N., Sezione di Milano Bicocca, Piazza della Scienza 3, 20126 Milano, Italy
[3] Faculty of Physics, University of Bielefeld, Universitätsstr., 33615 Bielefeld, Germany
[4] ECT*, strada delle tabarelle 286, 38100 Villazzano (Trento), Italy

Received: 25 April 2007 /
Published online: 6 June 2007 –

Abstract. We present a high order perturbative computation of the renormalization constants Z_V, Z_A and of the ratio Z_P/Z_S for Wilson fermions. The computational setup is the one provided by the *RI'-MOM* scheme. Three- and four-loop expansions are made possible by numerical stochastic perturbation theory. Results are given for various numbers of flavors and/or (within a finite accuracy) for generic n_f up to three loops. For the case $n_f = 2$ we also present four-loop results. Finite-size effects are well under control, and the continuum limit is taken by means of *hypercubic symmetric Taylor expansions*. The main indetermination comes from truncation errors, which should be assessed in connection with the convergence properties of the series. The latter is best discussed in the framework of boosted perturbation theory, whose impact we try to assess carefully. Final results and their uncertainties show that high-loop perturbative computations of lattice QCD renormalization constants (RCs) are feasible and should not be viewed as a second choice. As a by-product, we discuss the perturbative expansion for the critical mass, for which results are also for generic n_f up to three loops, while a four-loop result is obtained for $n_f = 2$.

1 Introduction

Lattice perturbation theory (LPT) has for a long time been the only available tool for the computation of lattice QCD renormalization constants (RCs). By now, non-perturbative computations are preferred. We should stress, however, that there is no theoretical obstacle to the perturbative computation of either *finite* or *logarithmically divergent* RCs, like, for example, those for quark bilinears or their ratios. The main difficulties are of a practical nature. The first one is that LPT is technically very hard, much harder than perturbation theory (PT) on the continuum; for a beautiful review on LPT, see [1]. Therefore, computations are often performed only at one loop. This is a serious limitation, which is made even more severe by the bad convergence properties of LPT. To take care of this problem, boosted perturbation theory (BPT) and/or of tadpole-improved perturbation theory (TIPT) [2] is often used. There is quite a consensus on the fact that at one loop the impact of BPT (and/or TIPT) is often important. On the other hand, there is no clear-cut result on the actual control on these procedures. One should always keep in mind that the convergence properties of the series are the real issue, and assessing them from a one-loop computation is of course impossible. Other improvement schemes have in recent years been proposed, which aim at resumming some leading contributions [3]. A different approach to the computation of RCs in lattice QCD is a completely non-perturbative one. In this case, one needs an intermediate scheme, which is eventually matched to the $\overline{\rm MS}$ scheme (the one in which phenomenologists are most interested in) by a continuum perturbative computation. Popular intermediate schemes are the regularization independent (RI'-MOM) [4] scheme and the Schrödinger functional (SF) [5] scheme. A non-perturbative computation eliminates the truncation errors. On the other hand, one needs to face all the difficulties inherent in the numerics. Among these is the high computational effort of unquenched (or partially quenched) lattice QCD simulations. In practice, it is sometimes extremely hard to get a good signal for realistic simulation parameters. For this reason LPT is still necessary, either for comparison, or because it is the only feasible approach.

In recent years, the technique of numerical stochastic perturbation theory (NSPT) has been introduced (for an extended introduction – which in particular covers the unquenched version – see [6]). NSPT is a numerical implementation of stochastic PT [7]. It is a numerical tool that enables one to perform LPT computations with no reference whatsoever to diagrammatics. By making use of NSPT we can compute lattice QCD RCs to high orders, which here means three (or even four) loops. At these

[a] e-mail: scorzato@ect.it

orders the use of BPT enables one to assess the convergence properties of the series and to gain better control of the truncation errors. Since we necessarily work on a finite lattice, finite-volume and scaling violation effects have to be assessed carefully: this can be done. A careful extraction of the continuum limit is one of the good points of the approach: the solution comes from what we call *hypercubic symmetric Taylor expansions*. Another nice feature comes from the fact that we can work directly in the massless limit (which is also where RCs are usually defined). This also eliminates the need of expensive chiral extrapolations. Finally, perturbative computations offer the possibility of stronger analytical control, knowing the dependence on the coupling and on the number of flavors.

The main message of this paper is that high-loop perturbative computations of lattice QCD RCs are feasible and should not be seen as a second choice. In particular, having both the perturbative and the non-perturbative determinations of RCs gives a valuable comparison. This is not at all academic. As a matter of fact, non-perturbative determinations are based on assumptions that have only been proved in PT.

This is the first of a couple of papers that deal with the NSPT perturbative computation of Wilson quark bilinears. Renormalization conditions are fixed by the RI'-MOM prescriptions. Here we can make a comparison with a non-perturbative determination [8].[1] In this paper we will concentrate on the determination of *finite* RCs: Z_V, Z_A and the ratios Z_P/Z_S and Z_V/Z_A [2] for (unimproved) Wilson fermions. As a by-product, we also obtain the expansion for the critical mass. Results are given for various numbers of flavors. At three loops some results are even given (to a finite accuracy) for generic n_f. Instead, we present fourth loop results for the $n_f = 2$ case only. A forthcoming paper will deal with the computation of logarithmically divergent RCs for quark bilinears (in particular, the RC for the scalar current $Z_S = Z_m^{-1}$, which is phenomenologically relevant for the determination of the quark masses). This deserves some extra caution, since dealing with anomalous dimensions requires one in particular to take care of finite-volume effects.

The paper is organized as follows. In Sect. 2 we recall the basic definitions of the renormalization scheme to which we adhere, while in Sect. 3 we discuss some technical details of our computations. Section 4 introduces the main tool that is needed to extract the continuum limit (the already mentioned hypercubic symmetric Taylor expansions): this is done by discussing the (prototype) computation of the quark propagator. Section 5 contains our results: first we discuss the finite ratios Z_P/Z_S and Z_V/Z_A, for which we can fit three-loop results for generic n_f; then we move to Z_V and Z_A (results are given at three loops for $n_f = 0$ and at four loops for $n_f = 2$); finally, we present a by-product of our computations, i.e. the critical mass to three loops (again, actually four in the case $n_f = 2$). In Sect. 6 we discuss the general features of computations dealing with an anomalous dimension (this sets the stage for what will be discussed in a following paper [9]). In Sect. 7 we deal with resummations and convergence properties of our series, and finally Sect. 8 contains our conclusions and perspectives for future applications.

2 The RI'-MOM renormalization scheme

In order to compute the renormalization constants we adhere to the RI'-MOM scheme. This is one of the so-called physical schemes[3] (as opposed to the more popular $\overline{\rm MS}$ scheme), and it goes back to the MOM scheme of [10]. It became very popular after the introduction of non-perturbative renormalization in [4]. RI emphasizes the *regulator independent* nature of the scheme, which in particular makes the lattice a viable regulator. The prime denotes a renormalization condition for the quark field, which is slightly different from the original one. All the details on this scheme can be found, for example, in [11]. In the following we only introduce the definitions that are relevant for our application.

The basic quantities of our computation are the quark bilinears between external quark states at fixed (off-shell) momentum p,

$$\int \mathrm{d}x \langle p|\overline{\psi}(x)\Gamma\psi(x)|p\rangle = G_\Gamma(pa)\,. \tag{1}$$

Here Γ stands for any of the 16 matrices that provide the standard basis of the Dirac space (Dirac indices will often be suppressed). We adopt the usual naming convention for the bilinears: the scalar (S) is defined by $\Gamma = 1$, the vector (V) by $\Gamma = \gamma_\mu$, the pseudoscalar (P) by $\Gamma = \gamma_5$, the axial (A) by $\Gamma = \gamma_\mu\gamma_5$ and the tensor (T) by $\Gamma = \sigma_{\mu\nu} = 1/2[\gamma_\mu, \gamma_\nu]$. Above, we made explicit the dependence on the lattice spacing a, which serves as a regulator. Below we will use the notation $\hat{p} = pa$.

These quantities being gauge dependent, a choice for the gauge condition has to be made. We will focus on computations in the Landau gauge. From a numerical point of view, this gauge condition is easy to fix on the lattice. Moreover, one does not need to discuss the gauge parameter renormalization. It also gives some extra bonus: the anomalous dimension for the quark field is zero at one loop.

We can trade the $G_\Gamma(pa)$ for the amputated function $\Gamma_\Gamma(pa)$ ($S(pa)$ is the quark propagator)

$$G_\Gamma(pa) \to \Gamma_\Gamma(pa) = S^{-1}(pa)G_\Gamma(pa)S^{-1}(pa)\,. \tag{2}$$

The $\Gamma_\Gamma(pa)$ are eventually projected on the tree-level structure by a suitable operator $\hat{P}_{O_\Gamma}$

$$O_\Gamma(pa) = \mathrm{Tr}\left(\hat{P}_{O_\Gamma}\Gamma_\Gamma(pa)\right)\,. \tag{3}$$

[1] The comparison will be made for given values of the coupling ($\beta = 5.8$) and number of flavors ($n_f = 2$).

[2] We will explain below why the computations of Z_V, Z_A and Z_V/Z_A are not tautological here.

[3] One should nevertheless keep in mind that the name *physical* is actually misleading in the case of QCD.

Renormalization conditions are now given in terms of the $O_\Gamma(pa)$ according to

$$Z_{O_\Gamma}(\mu a, g(a)) Z_q^{-1}(\mu a, g(a)) O_\Gamma(pa)\big|_{p^2=\mu^2} = 1\,. \qquad (4)$$

Here the Zs depend on the scale μ via the dimensionless quantity μa, while the dependence on $g(a)$ will be expanded in PT. One should keep in mind from the very beginning that we will eventually be interested in the $a \to 0$ limit of the Z. The quark field renormalization constant Z_q, which enters the above formula, is defined by

$$Z_q(\mu a, g(a)) = -\mathrm{i}\frac{1}{12}\frac{\mathrm{Tr}(\not{p} S^{-1}(pa))}{p^2}\bigg|_{p^2=\mu^2}\,. \qquad (5)$$

The original RI scheme (without a prime) would have a derivative with respect to p^μ, instead.

In order to get a mass independent renormalization scheme, one imposes renormalization conditions on the massless quarks. In perturbation theory this implies knowledge of the relevant counterterms, i.e. the values of the various orders of the Wilson fermions' critical masses. One- and two-loop results are known from the literature [12, 13]. The third (and fourth) loop have been computed by us as a (necessary) by-product of the current computations: the results are reported in Sect. 5 (the three-loop result in the $n_f = 2$ case has already been reported in [6]). Notice that the situation in the non-perturbative framework is more cumbersome with respect to staying in the massless limit. The determination of the critical mass is in a sense the prototype non-perturbative computation of an additive renormalization constant. As is well known, also this is a matter of principle: being a power-divergent renormalization, the critical mass itself cannot be computed in perturbation theory in the continuum limit. Still, from a numerical point of view the massless limit is always reached by an extrapolation procedure, which is usually a major source of error in the non-perturbative determination of RCs for lattice QCD.

A great advantage of working in the RI'-MOM scheme is that the relevant anomalous dimensions are known to three loops [11]. One is usually ready to admit that getting the logarithms is the *easy* part in the computation of a renormalization constant, while fixing the finite parts is the *hard* part of the work. As we will see, the situation is, to a certain extent, the opposite in the case of NSPT. We actually take for granted the logarithms (they are fixed by the choice of the scheme) and mainly concentrate on the computation of finite parts. As is discussed in Sect. 6, finite-size effects open anyway the backdoor to corrections to the logarithmic contributions. Three loops being the order to which anomalous dimensions are known, this is also the order at which we can push our computations for every observable that has a non-vanishing anomalous dimension. On the other hand, the finite RCs we will be concerned with in the present paper are in principle not constrained by anything but numerical precision, and that is why we pushed the computation of these quantities to an even higher order (four loops, at the moment).

3 Some technical details of our computations

The lattice formulation we use in this work is defined by the plain Wilson action for gauge fields and plain (i.e. unimproved) Wilson fermions. As we said, our computational tool is NSPT [6]. Here we only point out those technical details that are relevant to the present computation. In its actual implementation, NSPT shares a few ingredients that are common to any lattice simulation. The main peculiarity is the representation of the fields as an expansion in the coupling constant, i.e.

$$U_\mu(x) = 1 + \sum_{i=1}^{n} \beta^{-\frac{i}{2}} U_\mu^{(i)}(x)\,. \qquad (6)$$

As is apparent from the formula above, our preferred expansion parameter is the inverse of the lattice parameter $\beta = 2N_C/g_0^2$, N_C being the number of colors and $g_0 = g(a)$ the bare lattice coupling; thus $\beta^{-\frac{1}{2}}$ is proportional to g_0. In our case a three-loop computation requires $n = 6$, while for four loops (which is at the moment the maximum order for which we report results in the $n_f = 2$ case) one needs $n = 8$. The proliferation of fields results in the request of a bigger amount of memory than in ordinary (non-perturbative) lattice QCD simulations. It is of course relevant also in terms of computing power: the algorithm is dominated by order-by-order multiplications, i.e. the number of floating-point operations grows as $n(n-1)/2$. While this may seem to be a great overhead with respect to ordinary non-perturbative dynamics, this is actually not true. In particular, in unquenched NSPT (like in any fermionic simulation) the basic building block is the inverse of the Dirac matrix, for which the perturbative nature of the computation results in a *closed* recursive algorithm, which is fairly well implemented [6]. Moreover, as we will discuss later, there is no need to extrapolate to the chiral limit. As a result, NSPT fermionic computations are actually less demanding than non-perturbative counterparts.

As in many non-perturbative numerical computations, it is worth producing fairly decorrelated configurations and store them for different subsequent measurements. A 32^4 lattice (both at three and at four loops) fits well on an APEmille crate. At the same orders, a 16^4 lattice can be managed by small PC-clusters or even by a robust (but nowadays standard) PC. While the first case is treated by our TAO[4] codes, the second case is implemented in the framework of a by now well-established C^{++} NSPT package.

The number of flavors n_f enters the computations as a parameter, i.e. one has to perform different simulations for different n_f. In perturbation theory each order has a trivial polynomial dependence on n_f, so that one can fit the n_f dependence. The case of $n_f = 0$ has by now been simulated both on 16^4 and on 32^4 lattices: results have been used to assess finite-size effects. The unquenched cases have been simulated on the bigger (32^4) lattice: $n_f = 2$ is the case for which we have the largest number of configurations, while we also have several tens of configurations

[4] TAO is the APE-dedicated programming language.

for both $n_f = 3$ and $n_f = 4$. As a result, at the moment we are not going to quote every result for any n_f. In particular, four-loop results are at the moment only given in the case $n_f = 2$, for a reason that will become clear in a moment.

As already stated, one good feature of NSPT computations is the fact that one can stay at the chiral limit. As we have already pointed out, the computation of the Wilson fermion critical mass was in a sense the prototype computation of a non-perturbative (additive, in this case) renormalization constant. It is also the prototype of a power-divergent renormalization that cannot be safely computed in PT in the continuum limit. On the other hand, no numerical simulation can be performed at $k_{\rm critical}$ (we adhere to the common non-perturbative notation of quoting the hopping parameter rather than the mass of the quark): the chiral limit is always reached by means of a convenient chiral extrapolation.

In perturbation theory one corrects for the additive quark mass renormalization by order-by-order plugging in critical mass counterterms. This is exactly what we do in NSPT. We were ready to start our simulations straight away at three-loop order, which requires the knowledge of the critical mass up to two loops, and this is exactly what can be taken from the literature [12, 13]. Each subsequent order asks for an iterative procedure: one computes the critical mass at the nth order (from nth-order simulations) and then plugs it in the $(n+1)$th-order simulations. In particular, for the case $n_f = 2$ our determination of the three-loop critical mass was good enough to plug it into four-loop simulations. The statistics we collected for the other values of n_f are at the moment not sufficient to safely aim at the same accuracy.

The RI'-MOM scheme renormalization has been discussed in a generic covariant gauge [11]. We have already stated that our computations were performed in Landau gauge and stressed what the advantages of a such a choice are. From the point of view of computer simulations fixing the gauge to Landau in NSPT simply requires the order-by-order implementation of a well-known (FFT-accelerated) iterative procedure [6]. It is worth stressing that in the NSPT framework also a peculiar implementation of the Faddeev–Popov mechanism is possible (see [14] for an application): by the same trick as the one that enables us to treat the fermionic determinant we can manage the Faddeev–Popov determinant, without the inclusion of ghost fields. Still, we can perform our computations in any covariant gauge with gauge parameter $\xi \neq 0$, i.e. the Landau gauge is the only one that is not viable (apart from an extrapolation procedure). While the generic covariant gauge NSPT simulation has (moderate) computational overhead, Landau gauge fixing has a delicate issue in the numerical noise, which is introduced by the (order-by-order) iteration. We explicitly checked that this noise was not a great problem (of course FFT-acceleration is quite helpful in reducing the number of iterations needed to fix the gauge). In the end the advantages of computing in Landau gauge were not overtaken by the care that is due to keeping this noise under control.

We now come to a brief description of how we compute the observables of (1). Trivial algebra (i.e. creating external states with quark operators and Wick-contracting to obtain propagators) leaves us with the task of computing expectation values (i.e. asymptotic Langevin time averages) of the quantities

$$\sum_{q;\sigma\tau} M^{-1}_{\alpha p;\sigma q} \Gamma_{\sigma\tau} M^{-1}_{\tau q;\beta p} \tag{7}$$

(where M is the Dirac operator; α and β are external polarizations; σ and τ are other spin indices; p and q are momentum indices; color degrees of freedom are always suppressed in the notation). The index p in the inverse Dirac operator is singled out by placing a δ-like source at p in momentum space, with the right polarization and color index (more details in the following section). Notice that in this way not only the inverse is to be computed on a source (as usual), but one actually squeezes all the information out of the configuration. This has the advantage of working directly in momentum space, which is natural in our framework (every inversion of M comes as a result of a computation that goes back and forth from momentum space [6]. The only measurement that is a bit different is that of the conserved vector current,

$$\begin{aligned} V^c_\mu = 1/2 \, \big(& \overline{\psi}(x)(\gamma_\mu - 1) U_\mu(x) \psi(x+\mu) \\ & + \overline{\psi}(x+\mu)(\gamma_\mu + 1) U^\dagger_\mu(x) \psi(x) \big) \, . \end{aligned} \tag{8}$$

A little algebra shows that also in this case the measurement can be quite efficient by reverting to a convolution product.

A very important improvement of our statistics comes from exploiting hypercubic symmetry: all the measurements connected by a hypercubic symmetry transformation are averaged. The fluctuations associated to this average are taken into account for assessing errors. As a general rule for the different measurements involved in our calculations, the bootstrap method was the basic tool for the computation of the errors.

To conclude this section on our computational method, we should comment on our treatment of the zero modes. Any perturbative expansion of LQCD has to face the problem of regularizing the zero mode contribution to the functional integral, since the free propagator cannot be inverted in those points. How this applies to NSPT has been discussed in [6]. The most common approach is to remove the degrees of freedom associated with the zero modes [1, 15]. Although this prescription is not gauge invariant, such contributions are expected to vanish in the infinite-volume limit. We should remark that gauge invariant alternatives to this procedure exist. These involve the use of twisted boundary conditions [16] or the Schrödinger functional scheme [5]. While we plan to perform computations also in those schemes in the future, in the present work we have only considered the prescription in which zero modes are removed. We will come back to this issue in Sect. 6.

4 Hypercubic symmetric Taylor expansions: the case of the quark propagator

We now proceed to discuss in detail a prototype computation, i.e. the one-loop computation of the quark field renormalization constant. In practice, we are going to describe how we measure the quark propagator. We will thus make it clear what we mean by hypercubic symmetric Taylor expansions.

The section is intended as a prototype computation, so let us pin down the expected general form of the nth loop coefficient of a RC:

$$z_n = c_n + \sum_{i=1}^{n} d_i(\gamma) \log(\hat{p})^i + F(\hat{p}) \,, \quad (\hat{p} = pa) \,. \tag{9}$$

We have to look for a finite number (c_n), a divergent part that is a function of the anomalous dimensions γ, and irrelevant pieces, which we can expect compliant to hypercubic symmetry, and which are described by a suitable function F. We take the needed anomalous dimensions from the literature and we subtract their contribution. In particular, for a one-loop computation we simply need to subtract a simple log multiplied by the one-loop anomalous dimension (in this section we will completely ignore all the contributions coming from finite-size effects, to which we will come back in Sect. 6). After such a subtraction we need a convenient way to fit the irrelevant pieces given by $F(\hat{p})$. The example at hand is both instructive and simple: in particular, in Landau gauge the quark field has zero anomalous dimension at one loop, so it is simply required to get rid of $F(\hat{p})$ in order to get the constant c_n we are interested in.

We want to compute the two point vertex function (the inverse of the quark propagator) for a massless fermion. In the continuum limit we have

$$\Gamma_2\left(p^2\right) = S\left(p^2\right)^{-1} \,.$$

On the lattice we define the dimensionless quantity $\hat{p} = pa$ (in general we use the hat notation for dimensionless quantities). Furthermore, we also explicitly write the dependence on the coupling (and since we compute in PT we write β^{-1} rather than β):

$$\begin{aligned} a\Gamma_2\left(\hat{p}, \hat{m}_{\rm cr}, \beta^{-1}\right) &= aS\left(\hat{p}, \hat{m}_{\rm cr}, \beta^{-1}\right)^{-1} \\ &= \mathrm{i}\hat{\not{p}} + \hat{m}_{\rm W}(\hat{p}) - \hat{\Sigma}\left(\hat{p}, \hat{m}_{\rm cr}, \beta^{-1}\right) \,, \end{aligned} \tag{10}$$

where $\hat{m}_{\rm W}(\hat{p}) = \mathcal{O}(\hat{p}^2)$ is the (irrelevant) mass term generated at tree level by the Wilson prescription, $\hat{\Sigma}(\hat{p}, \hat{m}_{\rm cr}, \beta^{-1})$ is the dimensionless self-energy (which is $\mathcal{O}(\beta^{-1})$), and $\hat{m}_{\rm cr} = am_{\rm cr}$ is the critical mass (which is $\mathcal{O}(\beta^{-1})$ as well). Since chiral symmetry is broken by the Wilson regularization, also massless fermions generate a mass counterterm.

The first step is to compute the self-energy $\hat{\Sigma}$ from our NSPT simulations. To do that, we need the propagator $a\,S(\hat{p}, \hat{m}_{\rm cr}, \beta^{-1})$ in momentum space, i.e.

$$aS\left(\hat{p}, \hat{m}_{\rm cr}, \beta^{-1}\right)_{\alpha\eta} = \langle M^{-1}_{\alpha p;\eta p} \rangle = T^{-1} \sum_{t=1}^{T} M^{-1}_{\alpha p;\eta p}(t) \,,$$

where $M_{\alpha p;\eta q}$ is the full fermionic matrix. We explicitly write only the spin indices (α and η) and the momentum coordinates (p and q), while the color indices are left implicit. The symbol $\langle\rangle$ stands for the average over the gauge configurations, and the right hand side makes explicit the average over the Monte Carlo history of length T. This is performed as described in [6]. Here we only recall that our method – based on a discretized stochastic Langevin equation – also involves an extrapolation on the stochastic time discretization. We are interested in those elements of the inverse fermionic matrix that appear in the main diagonal in momentum space. This is obtained by "sandwiching" the fermionic matrix in a δ-like source vector in momentum space: $\xi^{(\alpha;p)}_{\sigma}(q) = \delta_{\alpha\sigma}\delta_{pq}$. The order-by-order inversion is then performed as described in [6].

Once $aS(\hat{p}, \hat{m}_{\rm cr}, \beta^{-1})$ is obtained, we average over all the components that are connected by hypercubic symmetry transformations. For each given momentum, we numerically (order-by-order) invert the 4×4 propagators[5]. Finally, we obtain the self-energy $\hat{\Sigma}(\hat{p}, \hat{m}_{\rm cr}, \beta^{-1})$, as in (10).

Now we turn to the analysis of the self-energy that we have obtained as above. It can be written as

$$\begin{aligned} \hat{\Sigma}\left(\hat{p}, \hat{m}_{\rm cr}, \beta^{-1}\right) = \hat{\Sigma}_{\rm c}\left(\hat{p}, \hat{m}_{\rm cr}, \beta^{-1}\right) + \hat{\Sigma}_{V}\left(\hat{p}, \hat{m}_{\rm cr}, \beta^{-1}\right) \\ + \hat{\Sigma}_{\rm other}\left(\hat{p}, \hat{m}_{\rm cr}, \beta^{-1}\right) \,. \end{aligned} \tag{11}$$

$\hat{\Sigma}_{\rm c}$ is the contribution along the (Dirac) identity operator. By this we mean that the trace over the spin indices is $(1/4)\mathrm{Tr}_{\rm spin}(\hat{\Sigma}) = \hat{\Sigma}_{\rm c}$. Similarly, $\hat{\Sigma}_V$ is the contribution along the gamma matrices:

$$\frac{1}{4} \sum_{\mu} \gamma_\mu \mathrm{Tr}_{\rm spin}\left(\gamma_\mu \hat{\Sigma}\right) = \hat{\Sigma}_V \,.$$

Finally, $\hat{\Sigma}_{\rm other}$ includes all contributions along the remaining elements of the Dirac basis. We are not interested in such (irrelevant) terms, which are easily projected out. Therefore, we will forget about $\hat{\Sigma}_{\rm other}$ in the following.

$\hat{\Sigma}_{\rm c}$ contains the contribution to the critical mass; in fact

$$\hat{\Sigma}\left(0, \hat{m}_{\rm cr}, \beta^{-1}\right) = \hat{\Sigma}_{\rm c}\left(0, \hat{m}_{\rm cr}, \beta^{-1}\right) = \hat{m}_{\rm cr} = am_{\rm cr} \,. \tag{12}$$

By restoring physical dimensions one can inspect the a^{-1} divergence of the critical mass: $a^{-1}\hat{\Sigma}_{\rm c}(0, \hat{m}_{\rm cr}, \beta^{-1}) = m_{\rm cr}$. We will come back to it in the following section. For the moment, we concentrate on $\hat{\Sigma}_V$, which we need to extract the quark field RC. If we make a Taylor expansion in powers of a, its most general form up to order $O(a^4)$ is

$$\begin{aligned} \hat{\Sigma}_V = \mathrm{i} \sum_{\mu} \gamma_\mu \hat{p}_\mu \Big(\hat{\Sigma}^{(0)}_V\left(\hat{p}, \hat{m}_{\rm cr}, \beta^{-1}\right) + \hat{p}^2_\mu \hat{\Sigma}^{(1)}_V\left(\hat{p}, \hat{m}_{\rm cr}, \beta^{-1}\right) \\ + \hat{p}^4_\mu \hat{\Sigma}^{(2)}_V\left(\hat{p}, \hat{m}_{\rm cr}, \beta^{-1}\right) + \dots \Big) \,, \end{aligned} \tag{13}$$

[5] Here, we use the fact that the propagator is color diagonal at any order in perturbation theory.

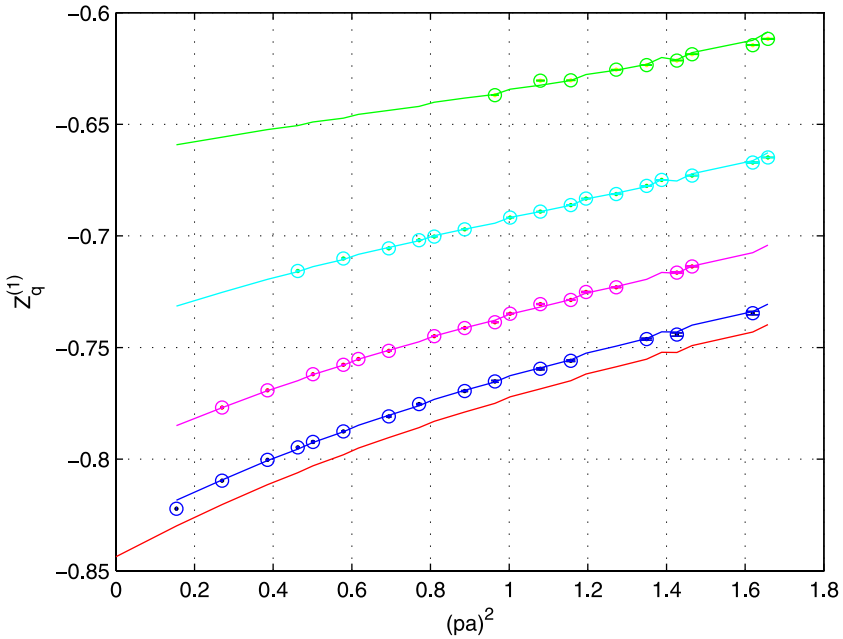

Fig. 1. The continuum-limit extrapolation of $Z_q^{(1)}$ (first loop of the quark field renormalization constant). We are interested in the intercept at $(pa)^2 = 0$, reached on the lowest line, which is the contribution $\hat{\Sigma}_V^{(0)}(\hat{p}, \hat{m}_{\rm cr}, \beta^{-1})$ in (13). The (*blue*, *violet*, *azure-blue*, *green*) *curves* represent the functions $\sigma(k, \hat{p})$ of (15) for $k = 1, 2, 3, 4$. The *red curve* is $\hat{\Sigma}^{(0)}$, which is only meant to guide the eye to the intercept at $(pa)^2 = 0$. The displayed fit includes up to $O(a^6)$ terms. Stability has been checked with respect to various numbers of terms and intervals

where the dots stand for higher terms in a. The functions $\hat{\Sigma}_V^{(i)}(.)$ (with $i = 0, \dots$), in turn, are the most general combinations of hypercubic invariant polynomials that contribute to the given order. In particular, the first term can be written as

$$\hat{\Sigma}_V^{(0)}\left(\hat{p}, \hat{m}_{\rm cr}, \beta^{-1}\right) = \alpha_1^{(0)} 1 + \alpha_2^{(0)} \sum_\nu \hat{p}_\nu^2 + \alpha_3^{(0)} \sum_\nu \hat{p}_\nu^4 + \alpha_4^{(0)} \sum_{\nu \neq \rho} \hat{p}_\nu^2 \hat{p}_\rho^2 + O(a^6)\,. \qquad (14)$$

For higher $i > 0$, there are of course less terms relevant for a given order. In general, all the possible covariant polynomials can be found through a character's projection of the polynomial representation of the hypercubic group onto the defining (four dimensional) representation of the same group (for a general reference, see, for instance, [17]).

To gain insight into (13), remember that in the free case the $\hat{\Sigma}_V^{(i)}$ correspond to the coefficient of $\hat{p}_\mu^{(i+1)}$ in the Taylor expansion of $2\sin(\frac{\hat{p}_\mu}{2})$. Equation (13) is what we call a hypercubic invariant Taylor expansion. The term in which we are interested is the leading term $\alpha_1^{(0)}$ in $\hat{\Sigma}_V^{(0)}$, since the other ones vanish in the continuum limit. In fact, the quark field RC Z_q is defined as (see (5); in the following we assume the color average has already been taken):

$$Z_q(\mu a) = \left. \frac{{\rm Tr}_{\rm spin}\left(\sum_\nu \gamma_\nu p_\nu \hat{\Sigma}_V\left(\hat{p}, \hat{m}_{\rm cr}, \beta^{-1}\right)\right)}{4ip^2} \right|_{p^2 = \mu^2}.$$

In order to explain in detail our fit procedure, let us define the auxiliary quantities

$$\sigma(k, \hat{p}) = \frac{1}{M} \sum_{\mu : \hat{p}_\mu = \frac{2a\pi}{L} k} \frac{{\rm Tr}_{\rm spin}\left(\gamma_\mu \hat{\Sigma}_V\left(\hat{p}, \hat{m}_{\rm cr}, \beta^{-1}\right)\right)}{\hat{p}_\mu} \qquad (15)$$

($L = Na$ is the linear size of the lattice). For a given momentum an average is taken over all the M directions μ such that $\hat{p}_\mu = \frac{2a\pi}{L} k$. For instance, consider the momentum $\hat{q} = (1, 1, 3, 2) 2\pi/N$. In this case $\sigma(1, \hat{q})$ has two contributions ($M = 2$): one from γ_1 and one from γ_2. Since also the $\sigma(k, .)$ are hypercubic invariant, they can be averaged accordingly. Referring to the example above, consider $\hat{t} = (3, 2, 1, 1) 2\pi/N$; symmetry requires that $\sigma(1, \hat{q}) = \sigma(1, \hat{t})$. In practice, they are averaged. Notice that the functions $\sigma(k, .)$ are specific linear combinations of the $\hat{\Sigma}_V^{(i)}$. In practice, we fit the data against the functions $\sigma(k, .)$. This is nothing but a fit of the constants entering the parametrization of $\hat{\Sigma}_V^{(i)}$ in (13). If we include $O(a^4)$ terms (as in (13)), we have to fit seven unknown constants. To order $O(a^6)$ we have 14 of these. We tried different orders up to $O(a^6)$ and checked the stability of the result. The interesting term is the leading one. Other coefficients have to do with irrelevant effects.

A nice illustration of the control that we have over our fits is provided by Fig. 1. There, we plot the functions $\sigma(k, \hat{p})$ up to $k = 4$, along with the curve $\hat{\Sigma}^{(0)}(\hat{p}, \hat{m}_{\rm cr}, \beta^{-1}))$, whose intercept in $\hat{p}^2 = 0$ is the parameter we are looking for. In Fig. 1 we choose to plot data versus $\hat{p}^2$, but one should keep in mind that this is not the only invariant under the hypercubic group entering $\hat{\Sigma}_V^{(i)}(\hat{p}, \hat{m}_{\rm cr}, \beta^{-1})$. Our numerical result reproduces very well the analytical one.

5 Results

In the previous section we saw an example with no anomalous dimension. This is of course also the case for finite RC (Z_V and Z_A) or finite ratios (Z_P/Z_S and Z_V/Z_A). In the following we present our results for these quantities. We computed at every order the relevant expectations values

dictated by (1). Finally, we performed the amputation and the projection on the tree-level structure. We could thus get the order-by-order expansions of the $O_\Gamma(pa)$ in terms of which RC are defined. The one-loop analytical results are well reproduced [18].

In the last subsection our results for the critical mass are presented.

5.1 The finite ratios Z_P/Z_S and Z_V/Z_A

The ratios Z_P/Z_S and Z_V/Z_A are safely computable at every order. This simply means to take (again, order-by-order) ratios of $O_\Gamma(pa)$ quantities. The quark field renormalization constant present in (4) drops out in the ratios, together with the divergence that affects Z_P and Z_S separately. In the end, one is left with the same situation we saw in the previous section: we simply have to perform at every order hypercubic invariant Taylor expansions to get the continuum limit coefficients of the expansions. One-loop examples are presented in Fig. 2. Fitting a scalar quantity like Z_P/Z_S is actually easier (there is no direction singled out and consequently only one function, to be fitted as a polynomial in the hypercubic invariants).

We could perform many checks on our results. Finite-size effects are well under control, as checked by comparing results on 16^4 and 32^4 lattices in the quenched case. In the next section we will elaborate on computations for which this is not the case. We also stress that we can compute both Z_A/Z_V and Z_V/Z_A; in the same way, we can compute both Z_P/Z_S and Z_S/Z_P. Due to the order-by-order nature of the computation, this is not a tautology: different ratios come from different (although correlated) combinations of data. We checked that to a very good precision the series obtained are inverses of each other.

Table 1 collects our results for different numbers of flavors. In the case $n_f = 2$ four-loop results are available. As already pointed out, the fact that we were able to go one loop higher is due to our better knowledge of the three-loop critical mass in the $n_f = 2$ case. Statistics in the cases $n_f = 3, 4$ is actually poorer. The fact that we could anyway go to three loops is a numerical accident: the signals for these ratios are actually very clean.

Table 1. The ratios Z_P/Z_S and Z_V/Z_A for various numbers of flavor n_f. Four-loop results are only available for $n_f = 2$

Z_P/Z_S				
n_f	$O(\beta^{-1})$	$O(\beta^{-2})$	$O(\beta^{-3})$	$O(\beta^{-4})$
0	−0.487(1)	−1.50(1)	−5.72(3)	n.a.
2	−0.487(1)	−1.46(1)	−5.35(3)	−21.6(3)
3	−0.487(1)	−1.43(1)	−5.13(3)	n.a.
4	−0.487(1)	−1.40(1)	−4.86(3)	n.a.
Z_V/Z_A				
n_f	$O(\beta^{-1})$	$O(\beta^{-2})$	$O(\beta^{-3})$	$O(\beta^{-4})$
0	−0.244(1)	−0.780(5)	−3.02(2)	n.a.
2	−0.244(1)	−0.759(5)	−2.83(2)	−11.5(2)
3	−0.244(1)	−0.744(6)	−2.72(2)	n.a.
4	−0.244(1)	−0.732(6)	−2.57(2)	n.a.

Having results for various numbers of flavors one can proceed to fit the n_f dependence. Since the polynomial dependence on n_f of every order is fixed, this is another test for our results (see Fig. 3). We got

$$
\begin{aligned}
(Z_P/Z_S)^{(2)} &= -1.50(1) + 0.0249(2) n_f \\
(Z_P/Z_S)^{(3)} &= -5.72(3) + 0.151(5) n_f + 0.0159(5) n_f^2 \\
(Z_V/Z_A)^{(2)} &= -0.780(5) + 0.0121(1) n_f \\
(Z_V/Z_A)^{(3)} &= -3.02(2) + 0.073(2) n_f + 0.098(3) n_f^2 \,.
\end{aligned}
$$

Presented in this (more universal) way the precision of our results appears to be a bit poorer. As expected, results are dominated by quenched contributions.

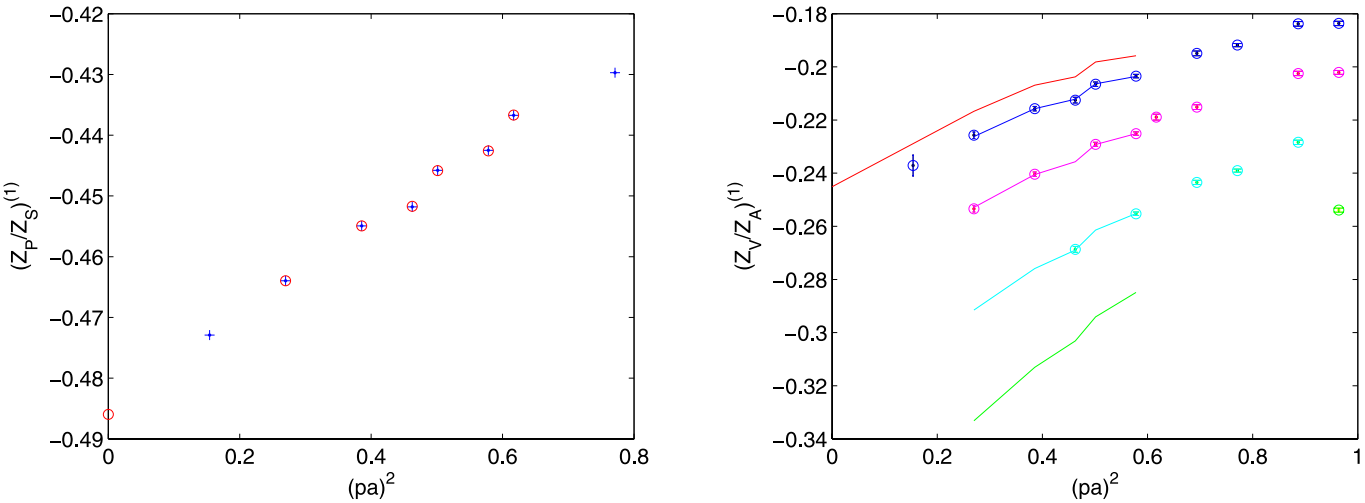

Fig. 2. Computation to one loop of finite ratios of the renormalization constants: Z_P/Z_S (*left*) and Z_A/Z_V (*right*). Data points taken into account in these particular fits are enclosed in *circles* (*left*) or joined by *solid lines* (*right*; see caption of Fig. 1)

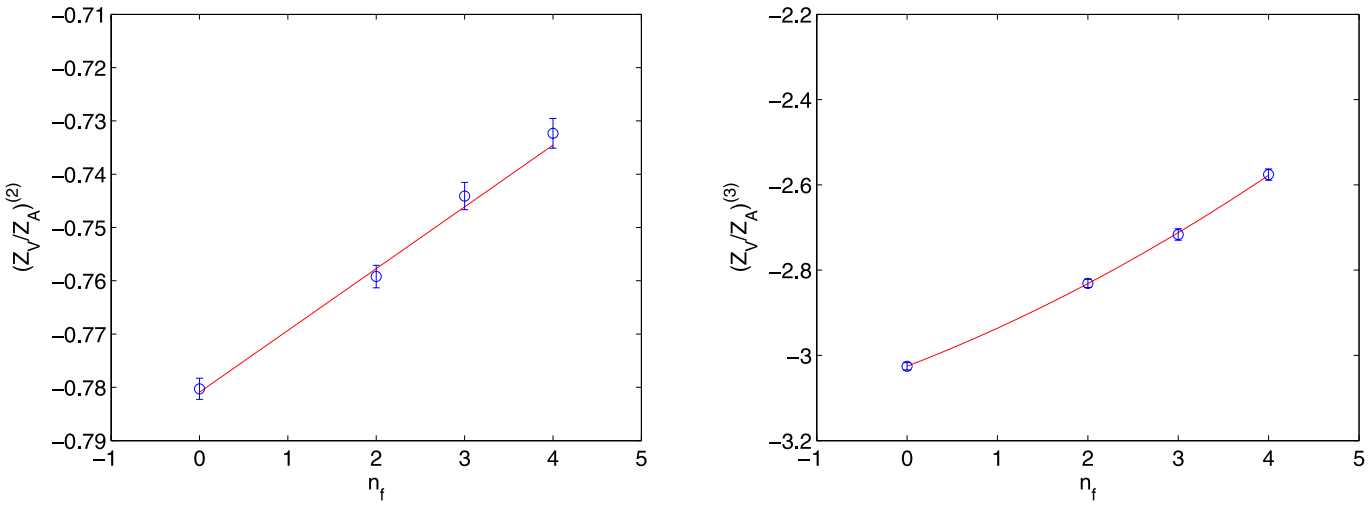

Fig. 3. The n_f dependence of the ratio Z_V/Z_A at two (*left*, linear fit) and three (*right*, quadratic fit) loops

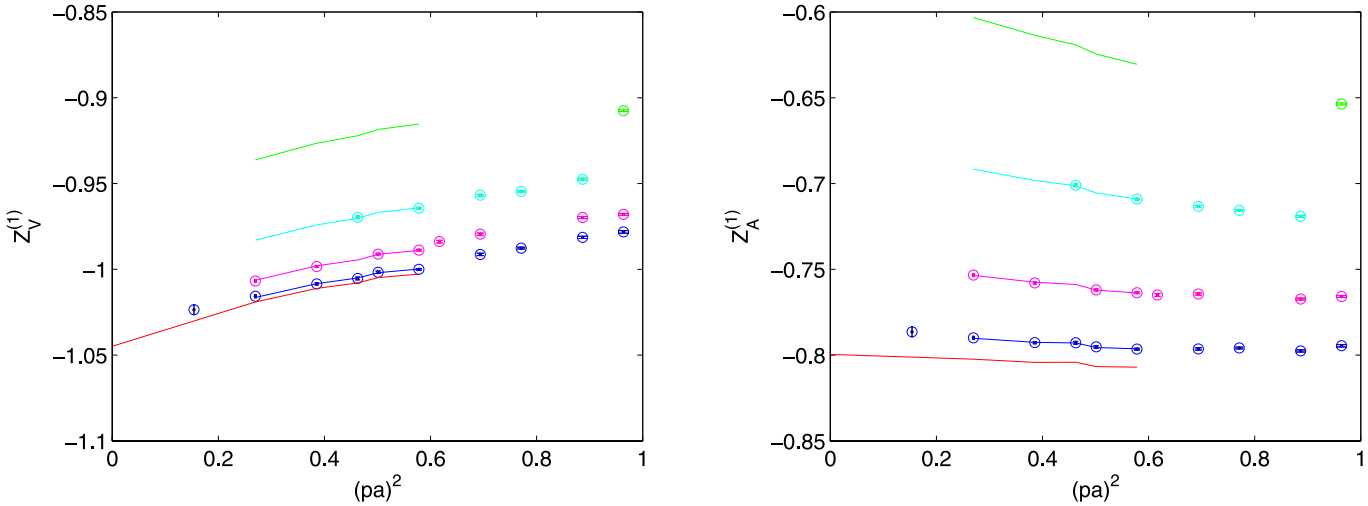

Fig. 4. Computation to one loop of finite renormalization constants: Z_V (*left*) and Z_A (*right*). Same notation as in Fig. 2

5.2 Z_V and Z_A

One-loop examples of computations of Z_V and Z_A are plotted in Fig. 4. Z_V and Z_A are finite quantities by themselves. In our master formula (4) they are interlaced with logs coming from the quark field renormalization constant. The latter can be eliminated in two different ways. A first strategy is to cancel Z_q directly from the measurements of the propagator. Another possibility is to take ratios with the conserved vector current: this is just what we did in the case of Z_P/Z_S and Z_V/Z_A, this time having one of the Z equal to one. Both procedures return consistent results, which are summarized in Table 2, where we present results for $n_f = 0, 2$ (also in this case, four-loop results are available for $n_f = 2$).

We have just discussed the two different approaches we used to compute Z_V and Z_A. In the previous subsection we presented results for the ratio Z_V/Z_A, which can of course as well be computed from the computation of Z_V and Z_A. One can verify that all these measurements are very well consistent. Still, they are controlled by different numerical noise, so that (for example) a direct computation of the ratio Z_V/Z_A is viable for all the n_f we took into account, while this is not the case for Z_V and Z_A separately (as already stated, statistics for $n_f = 3, 4$ is poorer). In the

Table 2. The finite renormalization constants Z_V and Z_A for $n_f = 0, 2$

Z_V				
n_f	$O(\beta^{-1})$	$O(\beta^{-2})$	$O(\beta^{-3})$	$O(\beta^{-4})$
0	−1.044(2)	−1.98(3)	−6.10(8)	n.a.
2	−1.044(2)	−1.88(3)	−5.42(8)	−17.0(9)
Z_A				
n_f	$O(\beta^{-1})$	$O(\beta^{-2})$	$O(\beta^{-3})$	$O(\beta^{-4})$
0	−0.800(2)	−1.39(3)	−4.04(4)	n.a.
2	−0.800(2)	−1.31(3)	−3.50(8)	−9.8(6)

Table 3. Three-loop critical mass for various n_f; a four-loop result is available for $n_f = 2$

m_{cr}	$n_f = 0$	$n_f = 2$	$n_f = 3$	$n_f = 4$
$O(\beta^{-3})$	$-13.11(6)$	$-11.78(5)$	$-11.02(9)$	$-10.24(9)$
$O(\beta^{-4})$	n.a	$-39.6(4)$	n.a	n.a

end, all these procedures differ from each other for different ways of fitting irrelevant contributions. Getting rid of irrelevant contributions to single out continuum limit results is a key issue in our approach, and so consistency between all these computations is a good test for reliability of our results.

5.3 A by-product: the critical mass

Analytical computations of the critical mass are available up to two loops [12, 13]. A three-loop computation in the $n_f = 2$ case was reported by our group in [6]. Here we present three-loops result for other n_f and add a four-loop result for $n_f = 2$. The results are collected in Table 3. They were obtained from the defining formula of (12) by fitting irrelevant contributions to $\hat{\Sigma}_{\rm c}(\hat{p}, \hat{m}_{\rm cr}, \beta^{-1})$. Also in this case there was no log coming from an anomalous dimension: in this case there is a power divergence, because of which a perturbative result is not to be taken as an accurate one. It is nevertheless valuable indeed to keep our fermions massless, i.e. as a counterterm.

Also in this case, one can fit a generic n_f result:

$$m_{\rm cr}^{(3)} = -13.11(6) + 0.62(5) n_f + 0.024(9) n_f^2 \,.$$

6 Dealing with anomalous dimensions

We anticipated that dealing with anomalous dimensions requires some extra care. In order to get some insight, we discuss a first example in which an anomalous dimension comes into place, i.e. the one-loop computation of Z_S. In this case our master formula (4) reads

$$\left(1 - \frac{z_q^{(1)}}{\beta} + \dots\right)\left(1 + \frac{z_s^{(1)} - \gamma_s^{(1)} \log(\hat{p}^2)}{\beta} + \dots\right) \times \left(1 + \frac{O_s^{(1)}(\hat{p}^2)}{\beta} + \dots\right)\Bigg|_{p^2=\mu^2} = 1 \,, \tag{16}$$

in which we explicitly wrote both the constant and the logarithmic contributions to the renormalization constants (the only log comes in this case from Z_S, since the one-loop quark field anomalous dimension is zero in Landau gauge). $O_s^{(1)}(\hat{p}^2)$ is what is actually numerically measured. At one-loop order we can solve the previous relation:

$$z_q^{(1)} - z_s^{(1)} = O_s^{(1)}(\hat{p}^2) - \gamma_s^{(1)} \log(\hat{p}^2) \,. \tag{17}$$

The message from (17) is simple: we will first subtract the logarithmic contribution and then proceed to our hypercubic invariant Taylor expansion. This is plotted in Fig. 5: upper data points are $O_s^{(1)}(\hat{p}^2)$, lower data points are the subtracted ones. We can see on the left of Fig. 5 that by going through this procedure we miss the analytical result. Notice that it looks like we were *subtracting too much*. To be definite, the subtracted data points bend quite a lot in the IR region. In the end, this does not come as a surprise: RI'-MOM is an infinite-volume scheme, but we are necessarily dealing with finite N (number of lattice points) computations. Since for $n_f = 0$ we have both 32^4 and 16^4 data, we are in a position to verify whether this is the real issue.

Figure 6 displays our results for $O_p^{(1)}(\hat{p}^2)$ (the equivalent of (17) for the pseudoscalar current), $O_s^{(1)}(\hat{p}^2)$ and of the ratio $\frac{O_s^{(1)}(\hat{p}^2)}{O_p^{(1)}(\hat{p}^2)}$ on the two different volumes. While the ratio (in the middle of the figure) is safe (we have already made this point in the previous section), quite remarkable finite-size effects are manifest for the $O_i^{(1)}(\hat{p}^2)$. It is obvious that by performing the subtraction of (17) on the 16^4 data points one misses the analytical result even more than in the left of Fig. 5. The picture stays much the same at higher loops.

It is in order to mention an important caveat. We have already made the point that our regularization of zero modes prescribes the removal of the degrees of freedom associated to them. This is a legitimate procedure in the $N \to \infty$ limit, which in turn means that we can have better and better approximations of infinite-volume results, but we cannot aim at having consistent perturbative expansions at a finite physical volume. Our aim is to single out the $N = \infty$ behavior, but this requires one to confront finite-N corrections, which we expect to be sizable in particular in the IR region.

One can define $L = Na$. Let us now write down for the quantity at hand the momentum sum $I(p, a, L)$ encoding the lattice Feynman diagram of the conventional Lattice perturbation theory, with the same ad hoc regularization of zero modes (zero momentum removed from the sum). Dimensional analysis suggests the presence of $pL = \hat{p}N$ effects (this relation holds for every value of a). In the spirit of the famous work [19] one can now split a (logarithmically divergent) Feynman diagram as in

$$\begin{aligned} I(p, a, L) &= I(0, a, L) + (I(p, a, L) - I(0, a, L)) \\ &\equiv I(0, a, L) + J(p, a, L) \,. \end{aligned} \tag{18}$$

We can now manipulate the momentum sums. The divergence is logarithmic, so by subtracting $I(0, a, L)$ we make $J(p, a, L)$ UV finite. Therefore, it can be computed (with the same ad hoc regularization of zero modes) in the $a \to 0$ limit. Although this does not define a finite-volume perturbative computation, it is a legitimate manipulation of the sum. In general, it will now be IR divergent, but this divergence (which is anyway regularized by finite L) will be canceled by contributions coming from $I(0, a, L)$, i.e.

$$\begin{aligned} I(0, a, L) &= c_1 + \gamma \log(a/L) + H(a/L) \\ J(p, a, L) &= c_2 + \gamma \log(pL) + G(pa, a/L, pL) \,. \end{aligned} \tag{19}$$

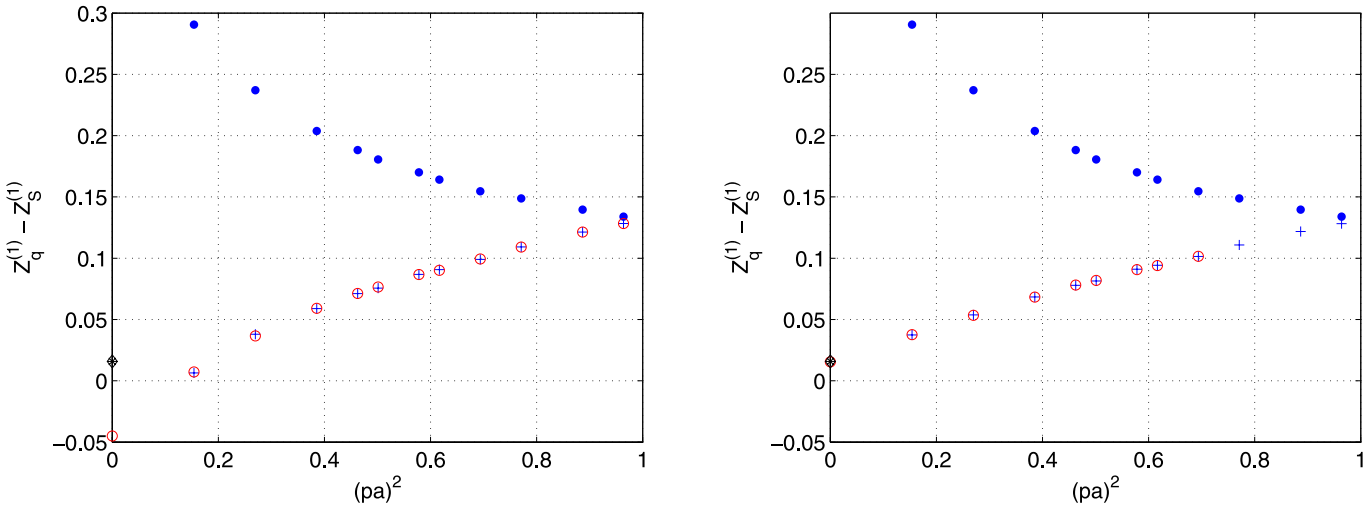

Fig. 5. Computation of one-loop renormalization constant for the scalar current. With respect to (17), *upper points* are the unsubtracted $O_s^{(1)}(\hat{p}^2)$, while *lower* (*circled crosses*) stand for the subtracted $O_s^{(1)}(\hat{p}^2) - \gamma_s^{(1)} \log(\hat{p}^2)$. An analytic result is marked with a *darker symbol*. On the *left*: no correction for finite volume. On the *right*: finite-volume tamed-log taken into account

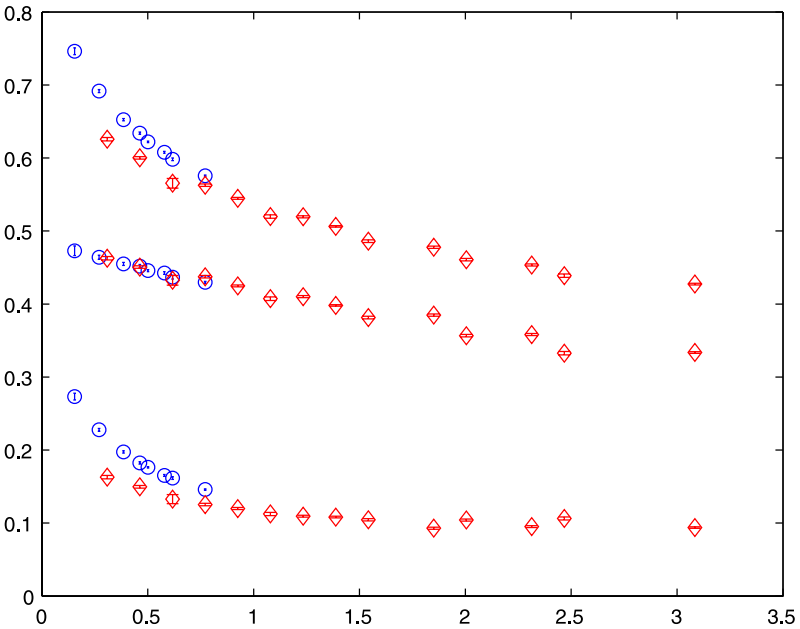

Fig. 6. Computations of $O_p^{(1)}(\hat{p}^2)$ (the equivalent of (17) for the pseudoscalar current) (*top*) and $O_s^{(1)}(\hat{p}^2)$ (*bottom*) on 32^4 (*circles*) and 16^4 (*diamonds*). In the middle is the ratio $\frac{O_s^{(1)}(\hat{p}^2)}{O_p^{(1)}(\hat{p}^2)}$, which appears safe with respect to finite-size effects

We point out that $I(0, a, L)$ cannot contain pL effects: these should be looked for in $J(p, a, L)$. Therefore, one can look for $pL = \hat{p}N$ effects in $G(pa, a/L, pL) \to \tilde{G}(pL)$. In order to obtain this quantity, we just computed the relevant graph in the formal continuum limit of our sum $J(p, a, L)$ ($a \to 0$ with $L = Na$ fixed), with the same ad hoc regularization of the zero modes. We call this contribution *tamed-log*, since it is supposed to resemble the expected log, but with $pL = \hat{p}N$ effects on top of it. We find that this function indeed approaches a log for $p \gg 1$. Figure 5 displays our results once one subtracts this tamed-log. As a matter of fact, if one stays away from deep IR the subtracted data points on the left and on the right of Fig. 5 are much the same. We stress that we are not saying that the finite-N effects we have just elaborated on are the only ones. By inspection, they appear to be the relevant ones, as it is confirmed by the fact that $N = 32$ and $N = 16$ now return the same results.

The situation is more complex at higher loops. We will devote to it a separate paper [9], in which we will explicitly gain information from different lattice sizes.

7 Resumming the series

We now go back to the expansions of Sect. 5.1 and Sect. 5.2 and try to resum them to obtain the finite RCs. Giving results and errors on top of them requires the estimates of the truncation errors. We will in the following adopt the strat-

egy of BPT. We stress from the very beginning that our real goal is to estimate the convergence properties of the series. It is only because of the sufficiently high order of the expansions that one can hope to really gain insight. One should nevertheless be ready to accept that every statement on convergence will be decided on by a strict case-by-case policy.

The different coupling constants we will use are all obtained in terms of the basic plaquette P. Let us define

$$x_0 = \beta^{-1}\,, \quad x_1 \equiv \frac{\beta^{-1}}{\sqrt{P}}\,, \quad x_2 \equiv -\frac{1}{2}\log(P)\,, \quad x_3 \equiv \frac{\beta^{-1}}{P}\,. \tag{20}$$

x_2 and x_3 are quite popular as boosted couplings. The reason why we also define x_1 will be clear in a moment. Obtaining the expansions in x_i once the expansions in x_0 are known is a textbook exercise, given the definitions in (20). One needs the expansion of the plaquette: analytical results [20] are only known to a given order, but our simulations always provide also the expansion of P.

We resum the series at $\beta = 5.8, n_f = 2$. This makes possible a comparison with the non-perturbative results of [8].

Figure 7 displays the resummation of Z_P/Z_S and Z_S/Z_P in the four different couplings. One can inspect from the very beginning the impact of a basic property of BPT that is often underestimated: all the couplings are equal at tree level, which means that all the expansions are equal at leading order. One-loop BPT amounts to sitting on a straight line, whose slope is dictated by the one-loop coefficient. Only at higher loops we can gain some insight on the convergence properties. There is actually a variety of convergence patterns (taking also x_1 into account is helpful in this respect).

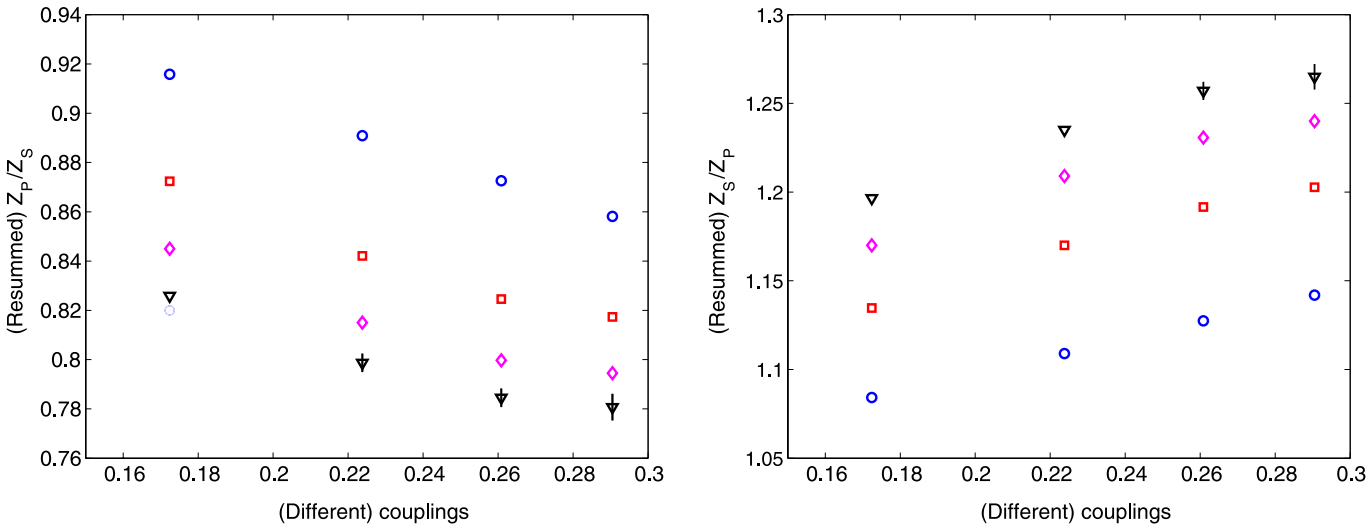

Fig. 7. Resummations of Z_P/Z_S (*left*) and Z_S/Z_P (*right*) for $n_f = 2$ at $\beta = 5.8$ to one (*circles*), two (*squares*), three (*diamonds*) and four (*triangles*) loops (the last is the only one that has a sizable error). We show resummations for different couplings: on the x-axis, the (different) values of the different couplings. From the left: x_0, x_1, x_2, x_3 (x_0 is β^{-1}; see text for the definitions of the other couplings)

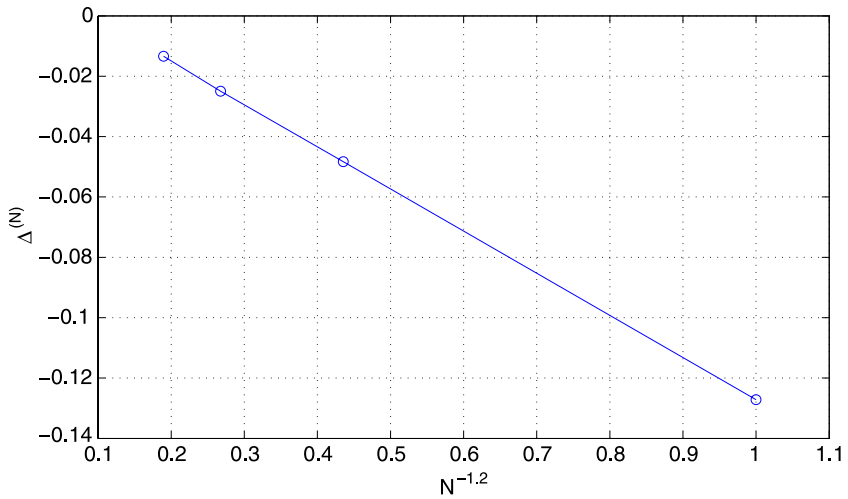

Fig. 8. The scaling of deviations of different order truncations for the quantity Z_P/Z_S for the x_2 coupling

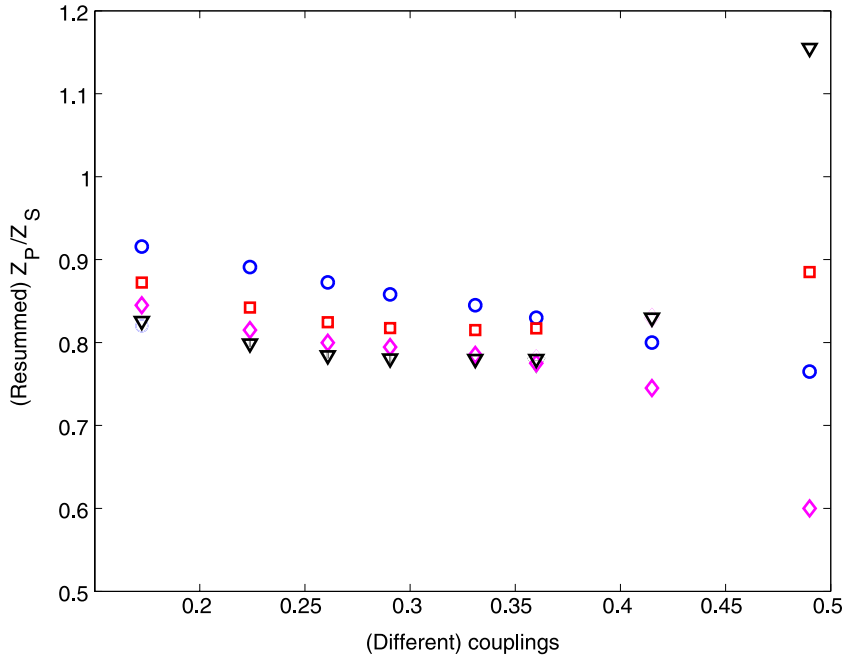

Fig. 9. Resummations of Z_P/Z_S (*left*) for $n_f = 2$ at $\beta = 5.8$. The same as in Fig. 7, but this time exaggerating the boosting of the couplings

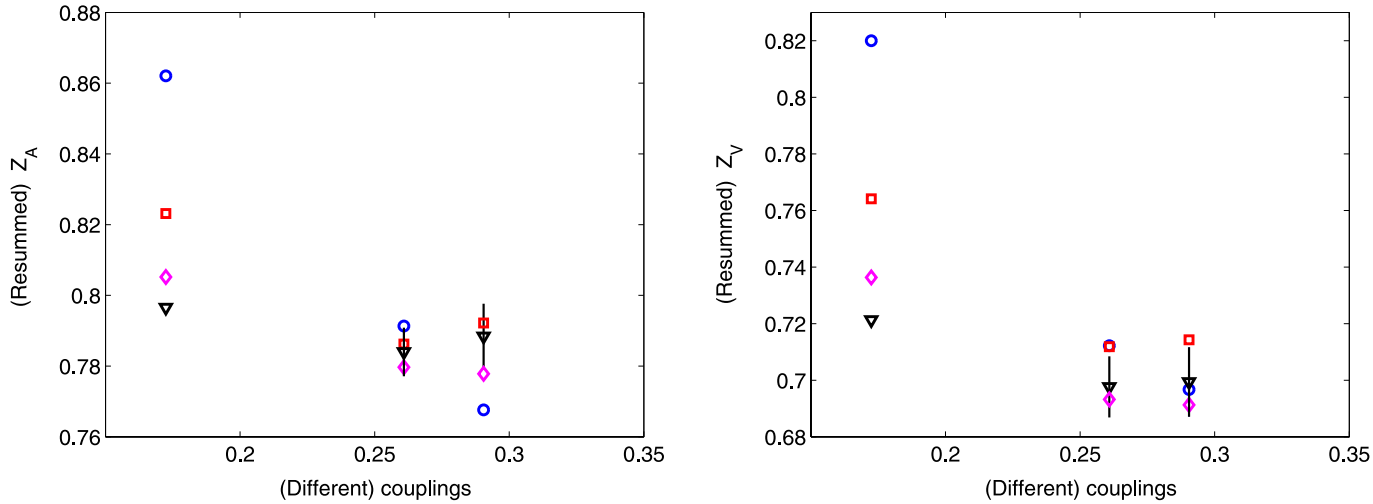

Fig. 10. Resummations of Z_A (*left*) and Z_V (*right*) for $n_f = 2$ at $\beta = 5.8$ to one (*circles*), two (*squares*), three (*diamonds*) and four (*triangles*) loops (the last is the only one that has a sizable error). We show resummations for different couplings: on the x-axis, the (different) values of the different couplings. From the left: x_0, x_2, x_3 (see text for the definitions of the couplings)

In particular, one can check the following.

- Within a fixed definition of the coupling, convergence is of course better and better as the order increases. As common wisdom suggests, convergence in the bare coupling is not so brilliant, and in general quite different convergence patterns are manifest; they appear to be quite satisfactory for x_2 and x_3. In particular, for the case of the x_2 expansion we plot in Fig. 8 the deviations $\Delta^{(n)}$, defined as the differences between resummation at order n and resummation at order $n-1$. The good scaling should not be taken too seriously (this is largely a numerical accident). Still, this signals a reasonable convergence pattern.
- As the order increases, expansions in different couplings get closer to each other, as expected; in particular expansions in x_2 and x_3 are quite close to each other.
- The resummed results for Z_P/Z_S and Z_S/Z_P in the x_2 and x_3 couplings are the inverses of each other to a reasonable accuracy. This is also a good indication.

Convergence properties of the expansions in the x_2 and x_3 couplings are good enough to extract a result. We notice that if one adds to the result at a given order the deviation from the immediately lower order, one always ends up at the same result (as a matter of fact a popular way to pin down a truncation error is just taken from the

deviations that we previously called Δ_n). We thus quote $Z_P/Z_S = 0.77(1)$.

We have already made the point that to assess the convergence properties one should adopt a case-by-case strategy. This can be clearly seen when we proceed to resum Z_A and Z_V. Before doing that, we give a trivial example of what a blind application of the idea of BPT can result in. In Fig. 9 we *exaggerate* the boosting of the coupling, by taking into account the other coupling $x_\alpha \equiv \frac{\beta^{-1}}{P^\alpha}$ ($\alpha > 1$). As one can see, the convergence properties are completely jeopardized.

In Fig. 10 we plot the resummation of Z_V and Z_A (again, at $\beta = 5.8, n_f = 2$). As one can see, this time the convergence properties of the expansion in the bare coupling are not so bad. Consequently, one is already at risk of overshooting at one-loop BPT, and the expansions in x_2 and x_3 would then oscillate. Our final estimates are $Z_A = 0.79(1)$ and $Z_V = 0.70(1)$.

Our resummed results are quite consistent with [8]. A greater deviation is seen on the values of Z_A and Z_V. To our understanding this could be mainly imputed to the indetermination coming from the chiral extrapolation.

8 Conclusions

We presented a high order computation of renormalization constants for lattice QCD. Finite-size effects are well under control for the quantities we considered. There is no extrapolation involved in staying at the chiral limit in which renormalization conditions are imposed. The continuum limit extraction is achieved in a clean way. Truncation errors can be well assessed by a judicious use of BPT. Thus, the main message of this paper is that high precision perturbative computations of lattice QCD renormalization constants are feasible and should not necessarily be regarded as a second choice.

Further work will follow, both to complete the job for logarithmically divergent quantities and to take into account different actions (in particular different fermionic regularizations). This is not expected to imply any change in strategy, and the implementation is mainly a matter of programming. In particular, work has already started to extend the results to Clover fermions and to other gauge actions.

Acknowledgements. We warmly thank Andrea Mantovi for having collaborated with us at an early stage of this project. We are very grateful to V. Lubicz and C. Tarantino for many stimulating discussions and for sharing with us their data. We also acknowledge interesting discussions with S. Capitani. F.D.R., V.M. and C.T. acknowledge support from both Italian MURST under contract 2001021158 and from INFN under i.s. MI11. L.S. has been partially supported by DFG through the Sonderforschungsbereich 'Computational Particle Physics' (SFB/TR 9).

References

1. S. Capitani, Phys. Rep. **382**, 113 (2003) [hep-lat/0211036]
2. G.P. Lepage, P.B. Mackenzie, Phys. Rev. D **48**, 2250 (1993) [hep-lat/9209022]
3. M. Constantinou, H. Panagopoulos, A. Skouroupathis, Phys. Rev. D **74**, 074503 (2006) [hep-lat/0606001]
4. G. Martinelli, C. Pittori, C.T. Sachrajda, M. Testa, A. Vladikas, Nucl. Phys. B **445**, 81 (1995) [hep-lat/9411010]
5. M. Luescher, R. Narayanan, P. Weisz, U. Wolff, Nucl. Phys. B **384**, 168 (1992) [hep-lat/9207009]
6. F. Di Renzo, L. Scorzato, JHEP **04**, 073 (2004) [hep-lat/0410010]
7. G. Parisi, Y.S. Wu, Sci. Sin. **24**, 483 (1981)
8. D. Becirevic, B. Blossier, P. Boucaud, V. Gimenez, V. Lubicz, F. Mescia, S. Simula, C. Tarantino, PoS(Lat2005) 079 [hep-lat/0509091]
9. F. Di Renzo, V. Miccio, C. Torrero, in preparation
10. W. Celmaster, R.J. Gonsalves, Phys. Rev. D **20**, 1420 (1979)
11. J.A. Gracey, Nucl. Phys. B **662**, 247 (2003) [hep-ph/0304113]
12. E. Follana, H. Panagopoulos, Phys. Rev. D **63**, 017501 (2001) [hep-lat/0006001]
13. S. Caracciolo, A. Pelissetto, A. Rago, Phys. Rev. D **64**, 094506 (2001) [hep-lat/0106013]
14. F. Di Renzo, M. Laine, V. Miccio, Y. Schroder, C. Torrero, JHEP **0607**, 026 (2006) [hep-ph/0605042]
15. U.M. Heller, F. Karsch, Nucl. Phys. B **251**, 254 (1985)
16. G. 't Hooft, Nucl. Phys. B **153**, 141 (1979)
17. W. Fulton, J. Harris, Representation Theory (Springer, Heidelberg, 1991), Graduate Texts in Mathematics **129**
18. G. Martinelli, Y.-C. Zhang, Phys. Lett. B **123**, 433 (1983)
19. H. Kawai, R. Nakayama, K. Seo, Nucl. Phys. B **189**, 40 (1981)
20. B. Alles, A. Feo, H. Panagopoulos, Phys. Lett. B **426**, 361 (1998) [Erratum-ibid. B **553**, 337 (2003)] [hep-lat/9801003]